Colloquium: Biophysical principles of undulatory self-propulsion in granular media

Daniel I. Goldman*

School of Physics, Georgia Institute of Technology, Atlanta, Georgia 30332, USA

(published 17 July 2014)

Biological locomotion, movement within environments through self-deformation, encompasses a range of time and length scales in an organism. These include the electrophysiology of the nervous system, the dynamics of muscle activation, the mechanics of the skeletal system, and the interaction mechanics of such structures within natural environments like water, air, sand, and mud. Unlike the many studies of cellular and molecular scale biophysical processes, movement of entire organisms (like flies, lizards, and snakes) is less explored. Further, while movement in fluids like air and water is also well studied, little is known in detail of the mechanics that organisms use to move on and within flowable terrestrial materials such as granular media, ensembles of small particles that collectively display solid, fluid, and gaslike behaviors. This Colloquium reviews recent progress to understand principles of biomechanics and granular physics responsible for locomotion of the sandfish, a small desert-dwelling lizard that "swims" within sand using undulation of its body. Kinematic and muscle activity measurements of sand swimming using high speed x-ray imaging and electromyography are discussed. This locomotion problem poses an interesting challenge: namely, that equations that govern the interaction of the lizard with its environment do not yet exist. Therefore, complementary modeling approaches are also described: resistive force theory for granular media, multiparticle simulation modeling, and robotic physical modeling. The models reproduce biomechanical and neuromechanical aspects of sand swimming and give insight into how effective locomotion arises from the coupling of the body movement and flow of the granular medium. The argument is given that biophysical study of movement provides exciting opportunities to investigate emergent aspects of living systems that might not depend sensitively on biological details.

DOI: 10.1103/RevModPhys.86.943 PACS numbers: 45.70.−n

CONTENTS

I. INTRODUCTION: LOCOMOTION IN THE NATURAL WORLD

Movement is an essential feature of any living system. It occurs across all biological time and length scales: transport of cargo along microtubules by transport proteins, fertilization of eggs by swimming spermatozoa, the beating of a heart, peristalsis during digestion, or the soaring of an eagle. For thousands of years (Aristotle, 350 BCE; Borelli, 1680; Alexander, 2003) scientists and engineers have worked to understand movement of a certain type: locomotion, or how organisms walk, run, and hop across land, fly through the air, and swim through water to feed, mate, and explore their environments. Laboratory and field studies of a variety of organisms (mainly by biologists, engineers, and mathematicians) have resulted in impressive understanding of the diversity of movement strategies across scales, including the bounding of kangaroos, soaring of birds, porpoising of dolphins, and the swimming of nematodes and spermatozoa; for a review, see Alexander (2003) and Cohen and Boyle (2010).

Studies of aerial and aquatic locomotion have provided ample opportunities for scientists, mathematicians, and engineers to interact (Vogel, 1994) since understanding such locomotion requires solving the equations of fluid flow, the Navier-Stokes equations (or using approximations). In such locomotion, the limb or body pushes against a medium that can itself move. Animals have evolved strategies for effective propulsion and lift within such materials, using limbs, bodies, and even heads to manipulate fluids. For example, a fruit fly creates lift and thrust through clap and fling shedding of vortices (Dickinson, Lehmann, and Sane, 1999), an eel accelerates fluid using an undulation of its body to generate thrust (Lauder and Tytell, 2006) through shedding of vortices, and a swimming *C. elegans* nematode worm operates in an environment in which inertia is not important [see reviews such as

*daniel.goldman@physics.gatech.edu

Lauga and Powers (2009) and Cohen and Boyle (2010)], and thus must use nonreciprocating motions (Purcell, 1977; Becker, Koehler, and Stone, 2003). Early work relied on analysis (Taylor, 1951; Gray and Hancock, 1955) with much work occurring at a low Reynolds number. This noninertial regime has proved a fruitful area of inquiry [for a review, see Lauga and Powers (2009)]; even gauge theory has been used to analyze such systems (Shapere and Wilczek, 1987). Recently computational fluid dynamics approaches have been used to numerically integrate the Navier-Stokes equations to predict locomotor performance of deforming shapes at higher Reynolds numbers (Tytell *et al.*, 2010). From a fluid physics point of view, flight and swimming have resulted in hundreds of years of challenging continuum mechanics (Childress, 1977; Vogel, 1994) questions which suggest, demand, and require new insights into the equations of motion for fluid flow.

In terrestrial locomotion, many studies focus on ground which presents a rigid, flat, and no-slip point contact interaction. By simplifying the ground interaction, unifying principles, like hopping while running (Cavagna, Heglund, and Taylor, 1977; Blickhan and Full, 1993) and vaulting while walking (Cavagna, Heglund, and Taylor, 1977), have been discovered and are obeyed by animals as small as cockroaches and as large as kangaroos. Recent laboratory experiments have begun to investigate the mechanisms of running on more complex surfaces. These include surfaces of varying stiffness (Ferris, Louie, and Farley, 1998; Spence *et al.*, 2010), surfaces that are highly dissipative (but do not flow) (Moritz and Farley, 2003), uneven (Daley *et al.*, 2006; Sponberg and Full, 2008), surfaces with few footholds (Bläsing and Cruse, 2004; Spagna *et al.*, 2007), surfaces with different inclination (Jayne and Irschick, 1999; Goldman *et al.*, 2006), and those that flow upon footsteps (Lejeune, Willems, and Heglund, 1998; Irschick and Jayne, 1999; Korff and McHenry, 2011; Li, Hsieh, and Goldman, 2012).

An area ripe for study is the movement of organisms on and within ground like sand, dirt, and mud which can flow, thereby challenging the simple categories of locomotion in fluid or solid environments. While there have been descriptive field-type studies, some investigators are beginning to examine such locomotion questions in detail using laboratory experiments and models (Dorgan *et al.*, 2005; Maladen *et al.*, 2009; Winter, Deits, and Hosoi, 2012), and the results are fascinating. Organisms encounter environments vastly different from those of pure fluids or solids—animals can make use of fluidlike, solidlike, and in some situations both, to move. One of the exciting challenges in this regime is that many such substrates are not yet described by equations of motion at the level of those for fluids, making analysis of locomotion problematic. Therefore, proceeding requires *simultaneous* advances in the biological physics of movement and the physics of intrusion in soft materials. These environments also present important practical challenges to robots which must slither (Hirose, 1993; Wright *et al.*, 2007) through debris to perform search and rescue (Murphy, 2014).

II. MODELING OF LOCOMOTION

Understanding locomotion requires not only experimental observation, but also modeling of the organism and the environment (Dickinson *et al.*, 2000; Holmes *et al.*, 2006). There have been attempts to describe organisms with complex [which include details of musculoskeletal and nervous systems (Zajac, 1993; Cruse *et al.*, 1998; Cofer *et al.*, 2010)] as well as simpler models (Blickhan, 1989; Kuo, Donelan, and Ruina, 2005). Certain behaviors (like walking and running on rigid ground) are amenable to simple, few-parameter models, which have the benefit that they can be understood through detailed analysis. For example, work on the nonlinear dynamics of running cockroaches has revealed that few-parameter ordinary differential equation models can describe and predict movement in both the sagittal (Seyfarth *et al.*, 2002) and horizontal (Schmitt *et al.*, 2002) planes. As with all biological problems however, a more detailed, integrative explanation requires an appropriate coupling of different scales of length, time, and complexity (Full and Koditschek, 1999). These low-order models therefore provide a starting point to understand the complexity from which locomotion emerges. That is, models at higher levels of complexity must reduce to simpler models. Simple models can also serve as "templates," targets of control (Full and Koditschek, 1999; Goldman *et al.*, 2006).

An increasingly useful tool to investigate animal locomotion is physical modeling—the use of robots that embody a feature of interest in the locomotor behavior (Koditschek, Full, and Buehler, 2004). Such devices can be used to test biomechanical and neuromechanical hypotheses (Ijspeert *et al.*, 2007; Lauder *et al.*, 2007; Nishikawa *et al.*, 2007) in environments that do not have to be (or cannot be) simulated. Low-cost off-the-shelf components have made construction of controllable robots relatively straightforward; such devices have the modeling benefit of interacting with real materials which might be undescribed (or possibly undescribable) by mathematical models. This is important: there are no fundamental models of legged robot interaction with rheologically complex terrain like sand and soil, and only recently have empirical "terramechanical" (Bekker, 1956; Wong, 1989) type approaches been successful in predicting locomotion on dry granular media (Li *et al.*, 2009, 2010; Li, Zhang, and Goldman, 2013).

III. LOCOMOTION AND BURIAL IN GRANULAR MEDIA

There is an entire living world beneath our feet (Wolfe, 2002), and much of the biomechanics of movement in such substrates is unknown (relative to movement in water, air, and on hard ground). Many species (and many undescribed organisms) move within soil, sand, and other flowable substrates which often deform during intrusion. These organisms range in size from tiny nematode worms (like *C. elegans*) (Gray and Lissman, 1964; Korta *et al.*, 2007; Jung, 2010) to earthworms (Darwin, 1897; Edwards, 1996) and ants (Hlldobler and Wilson, 1990; Tschinkel, 2006; Gravish *et al.*, 2013), to mice (Weber, Peterson, and Hoekstra, 2013) and moles. Even dry desert sand (Bagnold, 1941; Ezcurra, 2006), comprising roughly 10% of the Earth's surface, is home to a surprising number of organisms—from vertebrates such as camels, kangaroo rats, and sidewinder rattlesnakes to invertebrates such as solpugids and beetles. And fully saturated wet sand like that found at the shoreline and at the bottom of the ocean (Gray and Elliott, 2009) is home to many more

creatures whose locomotor biomechanics are largely unstudied, but which can operate quite effectively (Trueman, 1970; Dorgan, Arwade, and Jumars, 2007; Winter, Deits, and Hosoi, 2012).

Sand is an example of a dry granular medium (GM) (Jaeger, Nagel, and Behringer, 1996b), perhaps the simplest example of a complex substrate that can act as a fluid and/or solid. Many reptiles (e.g., lizards and snakes) can move both on and even within desert sand (Gaymer, 1971; Arnold, 1995); see examples in Fig. 1. A number of desert-dwelling lizards that are found in open dune environments (where they are often exposed to predators due to the lack of refuges like open burrows or vegetation) have evolved rapid submersion into sand as a mode of predator avoidance (Arnold, 1995).

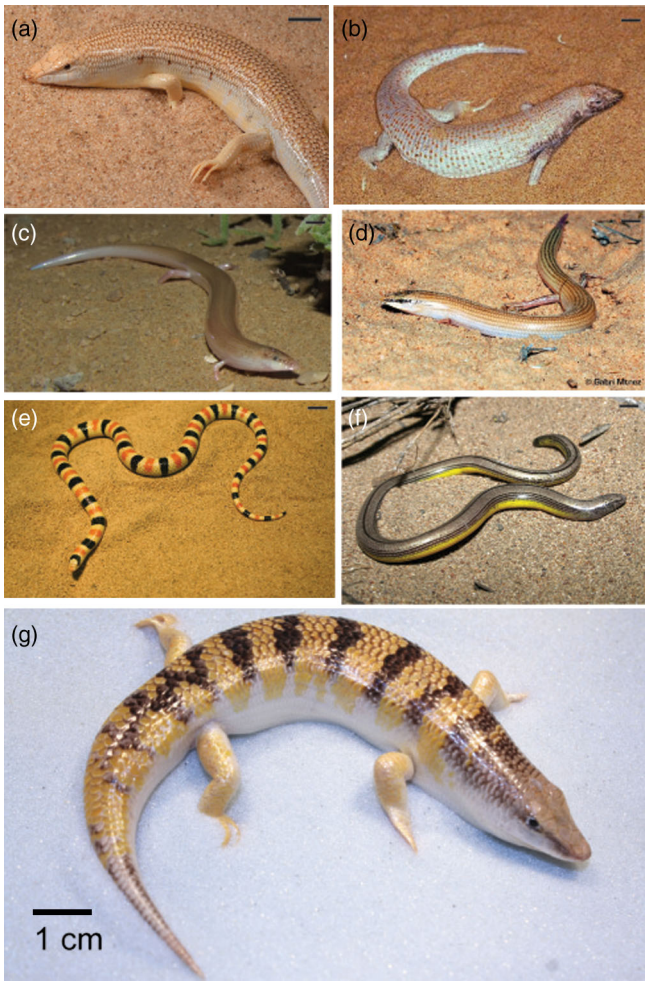

FIG. 1 (color online). A diversity of desert reptiles "swim" within dry granular media. (a) The Eastern sandfish *Scincus mitranus*. From Alexey Sergeev. (b) The desert plated lizard *Gerrhosaurus skoogi*. From Paul Freed, freedsphotography.com. (c) The three-toed snake skink *Ophiomorus tridactylus*. From Barbod Safaei Mahroo, CalPhotos. (d) The wedge-snouted skink *Chalcides sepsoides*. From Gabriel Martínez del Mármol Marín. (e) The Mojave shovel-nosed snake *Chionactis occipitalis*. From Perrin Schiebel. (f) The California legless lizard *Anniella pulchra*. From William Flaxington. (g) The Egyptian sandfish lizard *Scincus scincus*. From Sarah Sharpe. Scale bars in upper right of all panels denote approximately 1 cm.

Methods of rapidly burying in sand are varied: some animals enter the sand head first while others may sink vertically and, even when general modes of entry are similar, there may be marked differences in the way these are achieved and in the way the tail is finally concealed (Arnold, 1995).

Some lizards and snakes are classified as *subaranaceaous* indicating that not only do they bury, but they can also "swim" for distance within GM (Mosauer, 1932); see examples in Fig. 1. The Egyptian sandfish lizard (*Scincus scincus*) [Fig. 1(g)] is one of these. Observations from the field (Arnold, 1995) indicate that the animal uses limbs to run on the surface of the sand, but combines limb and body undulation to maneuver into sand. Once it is submerged in the material, it can move effectively (in our laboratory studies described below, at depths of up to 15 cm), although until our work described below, this behavior had never been visualized, and there had been no systematic study of the sand-swimming behaviors. The sandfish has several morphological features hypothesized to aid its locomotion in sand; these include a shovel-shaped snout and a countersunk lower jaw. It has been proposed that this latter structure reduces the drag on the shovel-shaped snout as the animal enters the material and protects the mouth from being forcibly opened when the animal moves through the sand (Mosauer, 1932).

IV. PHYSICS OF LOCALIZED INTRUSION IN GRANULAR MEDIA IN THE DENSE FLOW REGIME

The multibody interactions during burial and swimming of the sandfish generate new challenges in understanding granular flow (Andreotti, Bruno, and Pouliquen., 2013), an area of physics which has fascinated scientists (Jaeger, Nagel, and Behringer, 1996b) and engineers (Terzaghi, 1943) for many years. There has been much study of GM in the so-called rapid-flow regime (Jenkins and Richman, 1985; Campbell, 1990; Tan and Goldhirsch, 1998) in which particles do not experience enduring contacts, but instead interact purely through collisions. There have also been many studies of granular media globally forced at boundaries (Nedderman, 1992; Howell, Behringer, and Veje, 1999); these canonical tests can provide insight into material response to movement broadly, but are not often readily applicable to problems like those posed by the sandfish and other desert organisms. This is because unlike boundary-driven flows, in locomotor-relevant intrusions, an intruder forces itself through the medium such that only a small (and often nonsymmetric) region near the intruder is mobilized (fluidized) and material can resolidify after or even during transit.

This class of problems, which we call localized intrusions (Wieghardt, 1975; Albert *et al.*, 1999; Geng *et al.*, 2001; Hill, Yeung, and Koehler, 2005; Katsuragi and Durian, 2007; Goldman and Umbanhowar, 2008), are relatively unstudied [compared to boundary-driven triaxial loading tests (Nedderman, 1992; Andreotti, Bruno, and Pouliquen, 2013), for example]. There has, however, in recent years been interest in such problems. For example, although the impact of free, simply shaped bodies into granular media has been investigated for hundreds of years (Robins, 1742; Katsuragi and Durian, 2007; Goldman and Umbanhowar, 2008), from a physicist's point of view, much of the work has

been spent developing phenomenological models of intrusion; recently, this has changed however, as physicists seek fundamental microscopic principles associated with dynamics and energy dissipation mechanisms (Clark, Kondic, and Behringer, 2012).

Most relevant to the biological problem presented in this Colloquium on sand swimming, granular materials researchers have also studied horizontal intrusion (drag), where an object is towed through the medium at a fixed depth and fixed speed (see Fig. 2). The frictional nature of GM generates a yield force, a threshold below which grains do not flow in response to forcing (Nedderman, 1992). Once the yield force is exceeded and the material flows in steady state, in general, resistance forces depend nearly linearly on depth [see Fig. 2(b)]. At sufficiently low speeds (Albert *et al.*, 1999), unlike in fluids, resistance forces are independent of speed [see Fig. 2 and Albert *et al.* (1999), for example]. This is also largely a consequence of the frictional contacts between particles and intruder surfaces. Another interesting feature of granular drag is that it is insensitive to shape (Wieghardt, 1975; Albert *et al.*, 2001); thus streamlining has a modest effect relative to effects in fluids. However, while drag forces are insensitive to speed, vertical lift forces (perpendicular to the direction of motion) depend sensitively on shape and orientation of the intruding object (Ding, Gravish, and Goldman, 2011).

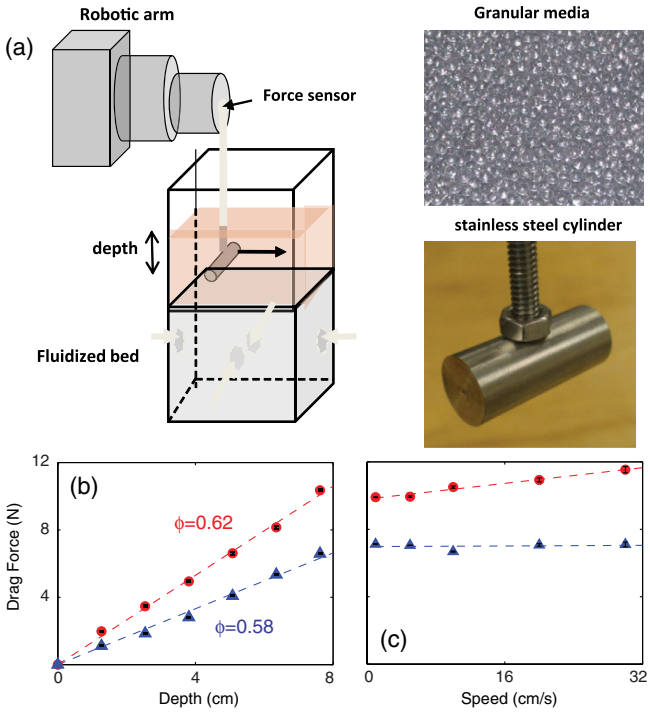

FIG. 2 (color online). Measuring drag forces in dry granular media. (a) A robotic arm moves a small horizontal cylinder (diameter 1.6 cm) within a fluidized bed of granular media (0.3 mm diameter glass particles shown); the air flow is used to prepare the substrate and is turned off during tests (Li *et al.*, 2009). Average drag forces during horizontal drag of the cylinder with axis oriented perpendicular to the drag direction through 0.3 mm diameter glass particles at (b) different depths below the surface and (c) at different drag speeds, at $\phi = 0.58$ and $\phi = 0.62$. The drag force from the support rod has been subtracted. (b), (c) Modified from Sharpe, Ding, and Goldman, 2012.

Dry GM can exist in different states of compaction characterized by the volume fraction ϕ, which is defined as the ratio of the total particle volume divided by the occupied volume. In natural dry granular environments composed of particles of roughly similar size (slightly polydisperse), ϕ can range from 0.57 to 0.64 (Dickinson and Ward, 1994). Little is known about how force and flow fields are created during localized movement in states that can dilate or consolidate in response to stress. In the laboratory, we studied the effects of ϕ on intrusion, primarily through the use of fluidized beds (see Fig. 2), devices in which a flow of air creates a fluidized granular state. Above a critical flow rate the pressure drop through the porous medium balances the weight of the grains and the granular media achieves a fluidized state in which enduring contacts between particles are no longer present. Rapidly halting the flow allows particles to settle into a loosely packed granular state. Higher ϕ states can be generated by mechanically vibrating the bed (Gravish, Umbanhowar, and Goldman, 2010) or pulsing air flow to the bed (Li *et al.*, 2009). We have generated such states in GM of slightly polydisperse ($\pm 15\%$) 0.3 mm diameter glass particles ranging in ϕ from 0.58 to 0.62. Average forces increased by nearly a factor of 2 over the small range of ϕ; see Fig. 2. As an interesting detail, we have found that above a critical volume fraction ($\phi \approx 0.6$) resistance forces transition from smooth in time to fluctuating (Gravish, Umbanhowar, and Goldman, 2010), a consequence of the periodic formation of "shear bands."

V. PHILOSOPHY

In this Colloquium I review my group's efforts to understand how the sandfish swims in sand; we bring the combination of visualization, muscle recording, and modeling tools (described below) to bear on this problem. I will illustrate how such locomotion problems require and benefit from the interplay of biological experiment, and mathematical, numerical, and robotic modeling. I also discuss how locomotion in granular media demands improved understanding of the mechanics of such materials; this is analogous to how the study of locomotion in fluids (e.g., air and water) has given insight into, and improved methods of modeling, relevant fluid flows. Finally I show how these approaches can be used to understand the neuromechanical targets of the control of organisms, revealing not just the "how," but also the "why" of movement. Whole organism studies, by focusing on emergent features (Anderson, 1972) of living systems, forces an inherently nonreductionist approach to science and engineering; this differs from the reductionist focus on "fundamental elements"; that is, if one understands the actions of the constituent elements, one can understand the whole. While movement certainly results from the combined action of many "microscopic" parts, it cannot be understood solely through the study of individual parts; after all, as I will show, animals and robots can share similar mobility despite being constructed from very different elements. As such, organism movement problems forces scientists and engineers to work together to discover what aspects of living

systems are details and what are basic principles. By working at the intersection of biology, robotics, and physics we can advance all three disciplines, and perhaps even create a synthesis, or a "consilience" in the words of the biologist E. O. Wilson (Wilson, 1998).

VI. SAND-SWIMMING MEASUREMENTS

A. Substrate preparation and movement visualization

To investigate how the sandfish moves within GM of different preparations, we developed a laboratory system to control properties of the substrate, image within it (Maladen *et al.*, 2009), and simultaneously record signals from muscles (Sharpe, Ding, and Goldman, 2013) responsible for bending. A schematic of the apparatus is shown in Fig. 3. It consists of a fluidized bed holding 0.3 mm glass particles with similar size and density (2.5 g/cm^3) to those found in natural desert environments.

Once the desired granular state is created (and the air flow is turned off), the animal is placed in a holding pen. A gate is lifted, the animal runs toward the sand, and rapidly dives in. High speed video cameras capture the above-ground locomotion kinematics. To visualize kinematics within the granular medium, we use x-ray imaging. X rays are emitted from a low energy source (approximately 160 kV and 20 mA) and transit through the granular bed (and animal). They are then collected by a tube-type image intensifier, which converts the x-ray photons to visible light photons which are recorded at up to 1000 frames/s by a high speed camera (Photron). Such devices are now at a low enough cost to utilize in laboratory experiments. The animal displaces sand; the minimum detectable contrast in pixel gray scales allows visualization of movement through approximately 15 cm of granular media. The apparatus is shown recording overhead (dorsal) images, but can also be rotated to record images from the side (sagittal) to visualize kinematics as a function of depth into the medium.

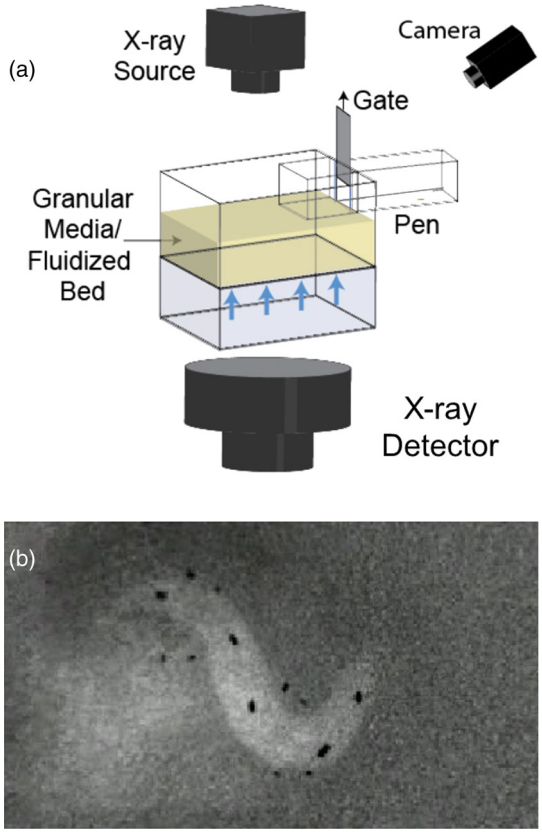

FIG. 3 (color online). (a) Experimental and visualization apparatus used to study sand swimming of the sandfish lizard, including fluidized bed to control the ϕ of the GM, and x-ray source and image intensifier detector to visualize movement within the GM. Adapted from Sharpe, Ding, and Goldman, 2012. (b) X-ray snapshot of the sandfish. Black spots are lead markers attached to the back and limbs of the animal.

B. Kinematic observations

The burial pattern is complicated and consists of movements of the limbs in concert with back undulation (Maladen *et al.*, 2009). Once the animal is fully submerged however, limbs are no longer used, and instead propulsion is generated using undulations of the back; see Fig. 4. To monitor the kinematics, we used computer software to track lead markers bonded to the scales of the animal on its midline and its limbs. We discovered that during its escape within the GM (which typically lasts 2–5 undulation cycles), to a good approximation (testing with approximately 20 animals), the undulation can be described as a single period sinusoidal wave traveling from head to tail down the body, such that

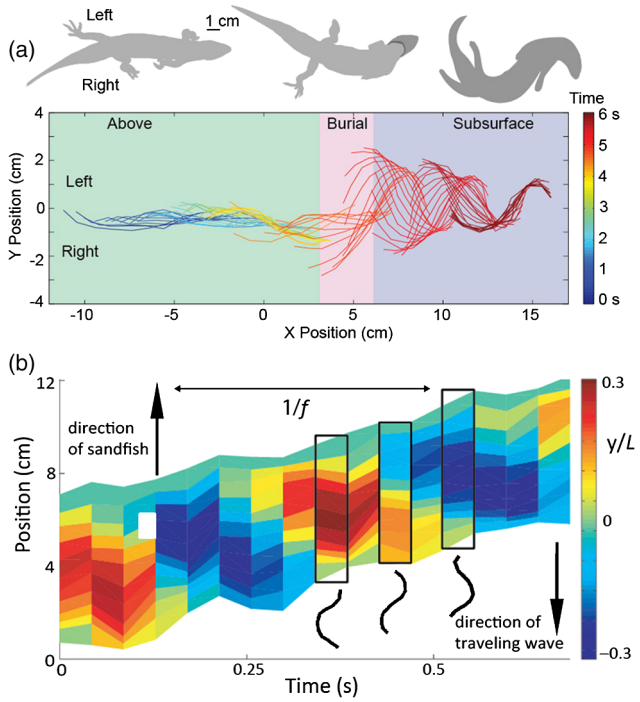

FIG. 4 (color online). Kinematics of undulatory sand swimming. (a) Time series of midline tracks during above-ground walking, burial, and subsurface swimming. Snapshots indicate typical body posture in these regions. Adapted from Sharpe, Ding, and Goldman, 2012. (b) Space-time plot of deviation of the body from a straight line during subsurface swimming, normalized by body length L. Black snapshots show tracked animal midline position and are well fit to a single period traveling sinusoidal wave. Adapted from Maladen *et al.*, 2009.

$$y = A \sin \frac{2\pi}{\lambda}(x + v_w t),$$

where y is the displacement from the midline of a straight animal and $v_w = f\lambda$; see the insets in Fig. 4(b), where f is the undulation frequency (set by the animal). The amplitude A and wavelength λ form a ratio A/λ which is insensitive to volume fraction ϕ and particle size (from 0.1 mm diameter glass particles to 3 mm glass particles) such that $A/\lambda \approx 0.2$; see Fig. 5. The animal increased swimming speed by increasing temporal frequency of the wave f; see Fig. 5. Remarkably, given the differences in resistance forces in different ϕ states, the slope of the relation is also independent of ϕ and particle size. Viewed from the side [data not shown, see Sharpe, Ding, and Goldman (2013) for details], the animal does not flex dorso ventrally and undulates in a plane inclined approximately 20° relative to the horizontal. It typically dives to a depth below the surface of 8–10 cm.

One important aspect of sandfish locomotion is the relationship of its average forward swimming speed v_x to the wave speed v_w. This ratio, obtained from the slope of the v_x/λ vs f plots in Fig. 5, is called the wave efficiency $\eta = v_x/v_w$ and for the sandfish is approximately 0.5 independent of ϕ and particle size. An $\eta < 1$ indicates that the animal does not advance as far forward as the wave advances in the backward direction and implies that the "tracks" of the midline are nonoverlapping (Fig. 4). For comparison, Fig. 6 shows η over a wide range of organisms, from those that crawl on a semisolid surface to larger animals that live in a fluid. The sandfish has an η between low Reynolds number swimmers and surface crawlers. Kinematically, the sandfish does not resemble water swimmers of its size [like salamanders and newts (Frolich and Biewener, 1992; Gillis, 1997; Ijspeert *et al.*, 2007) which increase the amplitude of the traveling wave down the body from head to tail], but more closely resembles the *C. elegans* nematode worm which lives in soil and whose locomotion has been studied in fluids of varying viscosity (Korta *et al.*, 2007) and viscoelasticity (Shen and Arratia, 2011), and in saturated particulate substrates (Juarez *et al.*, 2010; Jung, 2010). The η of the sandfish, however, is nearly double that of the nematode (Gray and Lissman, 1964) swimming in Newtonian fluids.

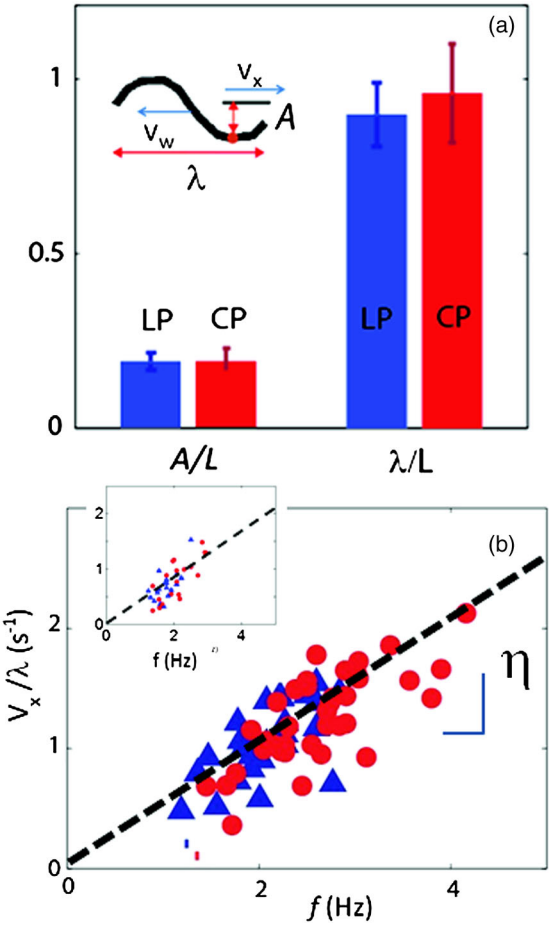

FIG. 5 (color online). Independence of swimming kinematics on substrate properties. (a) Spatial kinematics of the undulatory wave during sand swimming in 0.3 mm diameter glass particles. LP bars indicate loosely packed GM at $\phi = 0.58$, and CP bars indicate more closely packed GM at $\phi = 0.62$. The inset shows a tracked midline of an animal and quantities of interest. (b) Average forward swimming speed normalized by λ vs undulation frequency f in slightly polydisperse 0.3 mm diameter glass particles of $\phi = 0.58$ (triangles) and $\phi = 0.62$ (circles) and in 3 mm diameter glass particles (inset).

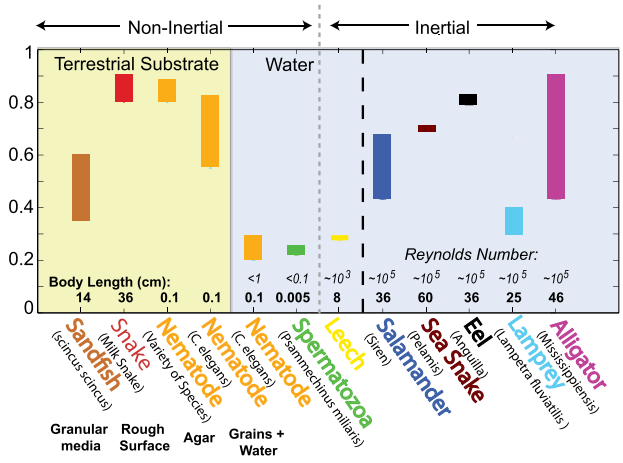

FIG. 6 (color online). Wave efficiencies η for a diversity of swimmers and crawlers. Data are collected from the following sources: Taylor (1952), Gray and Hancock (1955), Gray and Lissman (1964), Fish (1984), Gillis (1996), Maladen *et al.* (2009), Jung (2010), and Sharpe, Ding, and Goldman (2013).

VII. MODELING APPROACHES

In this section, I describe our approaches to the modeling of locomotion with the goal to explain how (and potentially why) the animal swims as it does. We are presented with an interesting (and circular) challenge. To understand sand swimming, we need a model of the organism and a model of the environment. If we assume that the organism model is simple such that it seeks to control its body to undulate in a particular pattern (template), we can ignore the internal biological complexity. We are then left needing a model of the environment. As noted in the Introduction, models of locomotion in true fluids (such as water and air) have been extensively studied (Childress, 1977; Vogel, 1994), a consequence of the long history of collaboration of biologists with physicists, mathematicians, and engineers. However,

granular media do not yet have a partial differential equation (PDE) description at the level of those for fluids, so our modeling has taken three approaches, each having its own specific benefits and shortcomings.

A. Discrete element method modeling

The first modeling approach relies on a technique utilized often in granular flows, that of multiparticle simulation, called the discrete element method (DEM) or soft-particle molecular dynamics (Rapaport, 2004; Poschel, 2005). In our three-dimensional (3D) DEM simulation, a computer program tracks the movements of millions of spheres under gravitational and contact forces. When particles or objects come into contact, they repel each other; see Fig. 7. To compute particle-particle and body-particle interaction forces, we calculated the normal force (Lee and Herrmann, 1993) F_n and the tangential Coulomb friction force F_s (see Fig. 7) at each contact using

$$F_n = k\delta^{3/2} - G_n v_n \delta^{1/2}, F_s = \mu F_n, \quad (1)$$

where δ is the virtual overlap between contacting objects, v_n is the normal component of relative velocity, and k and G_n represent the hardness and viscoelastic constants, respectively. μ refers to the particle-particle (μ_{pp}) or body-particle (μ_{bp}) sliding friction coefficients (we do not include static friction in this model). We can simulate different GM, including a 50:50 bidisperse mixture of 3.4 and 3.0 mm particles to approximate the size distribution of a real medium consisting of 3.2 ± 0.2 mm diameter glass particles (Maladen, Ding, Kamor *et al.*, 2011), and 6 mm plastic particles for robot experiments (see below).

Maladen, Ding, Kamor *et al.* (2011) validated the simulation (Fig. 7) by comparing the forces on a cylindrical stainless steel rod (see Fig. 2) dragged horizontally at different orientation angles relative to the cylinder axis within the simulated GM and those from drag experiments within the real medium. In the simulation of 3 mm diameter glass particles, the container holding the particles was $35 \times 15 \times 10$ cm^3 in volume and the initial volume fraction was set as 0.60 [see Ding, Gravish, and Goldman (2011) for preparation details]. Parameters in the particle-particle interaction model were adjusted until drag forces matched at a particular experimental condition [see (Maladen, Ding, Kamor *et al.* (2011) for details]. Remarkably, without changing these parameters, the validated model was able to predict forces on intruders over a wide range of experimental conditions in 3 mm glass particles, as well as 6 mm diameter plastic particles discussed below.

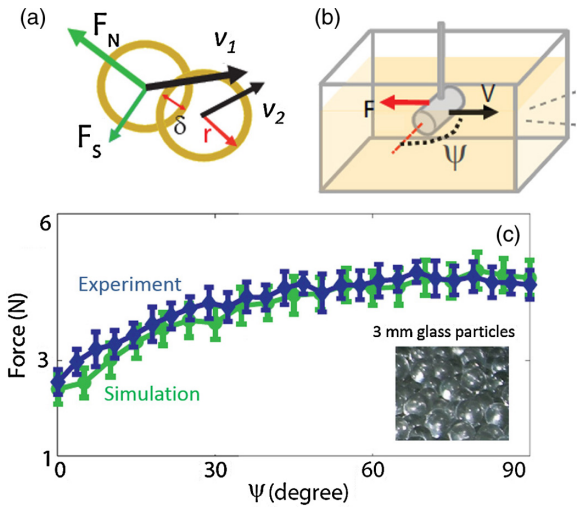

FIG. 7 (color online). The discrete element method (DEM) simulation of GM. (a) Particle-particle interaction demonstrating virtual overlap which determines normal F_n and tangential F_s forces for a two-particle collision. The vectors v_1 and v_2 refer to incoming velocities of the two particles and δ the virtual overlap. (b) Schematic of apparatus to validate the DEM simulation. (c) Average force vs orientation angle of a horizontal cylinder (the same cylinder as used in Fig. 2) during constant speed drag in experiment and simulation.

Once the GM simulation was established, a model of the organism was constructed; see Fig. 8 and Maladen, Ding, Kamor *et al.* (2011) for details. The sandfish was simulated using the commercial software package WORKING MODEL 2D (Design Simulation Technologies). The model sandfish was divided into 50 segments along its length. The segments were connected by actuators, which did not directly interact with the particles. The angle of each actuator was specified as a function of time such that an approximately single period sinusoidal wave (as observed in the animal experiments) traveled from head to tail. The simulation generated the necessary torques to maintain the body in the targeted waveform; as we discuss, all torques and powers were within physiologically reasonable limits (Ding *et al.*, 2012).

The DEM simulation could not simulate the natural sand in which the sandfish swims, since in a typical experimental container this would require an enormous number of particles (order 10^9) and using our current codes on desktop PCs would take months (although our recent porting of our code to GPU processors has led to significant decreases in computation time). Since the sandfish swims with $\eta \approx 0.5$ and $A/\lambda \approx 0.2$ over a wide range of particle sizes including 3 mm glass particles, we could simulate conditions close to the animal experiment.

The simulation captured the kinematics of the sand swimming: as in the biological experiments, the simulated sandfish swam with nonoverlapping midline trajectories [cf. Figs. 8(d) and 4(a)] when the wave amplitude A was set such that $A/\lambda = 0.22$ [based on animal observations (Maladen *et al.*, 2009)]. Further, as in the biological experiments, the simulated sandfish increased forward swimming speed with increasing undulation frequency, and the η was close to 0.5 and insensitive to the volume fraction of the simulated medium (see Fig. 11). In both experiment and simulation, due to the coupling of the body wave to the medium, trajectories of markers attached to the body appeared as distorted waves [not shown here, see Ding *et al.* (2012) for details]. The simulation rapidly (within one cycle) achieved a steady-state swimming pattern, indicating the unimportance of inertial effects of material or body segments.

Part of the strength of the simulation lies in its ability to reveal features of sand swimming, including the flow field near the swimmer, the reaction forces generated during locomotion, and power used to swim. All of these are challenging to measure in experiment. For example, it is a

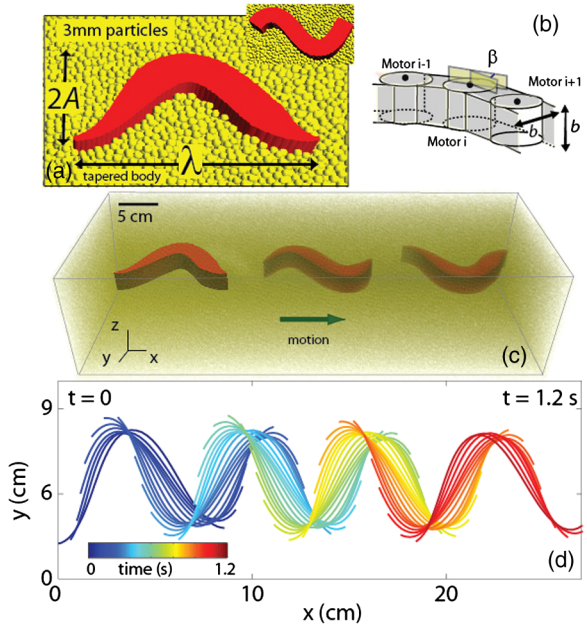

FIG. 8 (color online). Numerically simulated sandfish model of the animal. (a) Close-up view of the numerical sandfish with tapered body cross section (approximating that of the animal) in 3 mm simulated glass particles (particles above the sandfish model are rendered transparent). The inset shows the numerical sandfish with uniform body cross section, used to compare to RFT. The body length and height of the model sandfish were 12 and 1.6 cm, respectively. The mass of each segment was proportional to the cube of its width and the total weight of the simulated sandfish was 14 g. (b) Motor connections of a section of the simulated sandfish ($i = 1$ refers to the head). b indicates the width (maximum along the model) and height of the segments in the nontapered section of the animal model. (c) 3D view of a simulated sandfish at three different instants while swimming within a container of particles rendered semitransparent for visualization. The time taken by the simulated tapered head sandfish to swim across the container is approximately 3.5 s ($f = 2$ Hz). (d) Midline kinematics of simulated tapered sandfish with $f = 2.5$ Hz. Adapted from Maladen, Ding, Kamor *et al.*, 2011.

challenge to spatially and temporally resolve flow fields experimentally in the opaque granular medium in 3D [for information on techniques used to record flow fields in fluids using particle image velocimetry, see Willert and Gharib (1991)]. However, using the simulation, analysis of the flow field around the sand swimmer in simulation revealed that only in a region near the swimmer did particles have appreciable speed and were thus in a fluidized state; see Fig. 9(a). Inside the granular medium, the energy was dissipated due to the interaction forces and relative motion between particles. The so-called "granular temperature," which measures the deviatoric portion of the velocity field, can be used as an indicator of energy dissipation and fluidity of the local material (Jaeger, Nagel, and Behringer, 1996a, 1996b); the notion of granular temperature has proved useful in hydrodynamiclike descriptions of granular media (Jenkins and Richman, 1985; Shattuck *et al.*, 1999). We used the definition of granular temperature as $\langle (u - \langle u \rangle)^2 \rangle$ as in Campbell (1990), where u is the particle velocity and "$\langle\,\rangle$" denotes averaging over cells at the same depth of the model sandfish. As shown in Fig. 9(b), high temperature regions appeared only in the vicinity of the body and also decayed to nearly zero within a distance of about the diameter of the body. The localized high temperature regions indicate the swimmer can fluidize only a limited volume of granular material and energy is dissipated locally.

The simulation allowed the analysis of the energetic cost to break frictional contacts and maintain the localized fluid. From torque generated during the movement of segments, we measured the power to swim and found that within the range of animal swimming frequency, the average power increased linearly with frequency (and power was in physiologically reasonable ranges for muscle); see Fig. 9(c). This implies that, unlike movement in true fluids, the force to swim is insensitive to frequency. Indeed, using the simulation to make the first prediction of sand swimming reaction

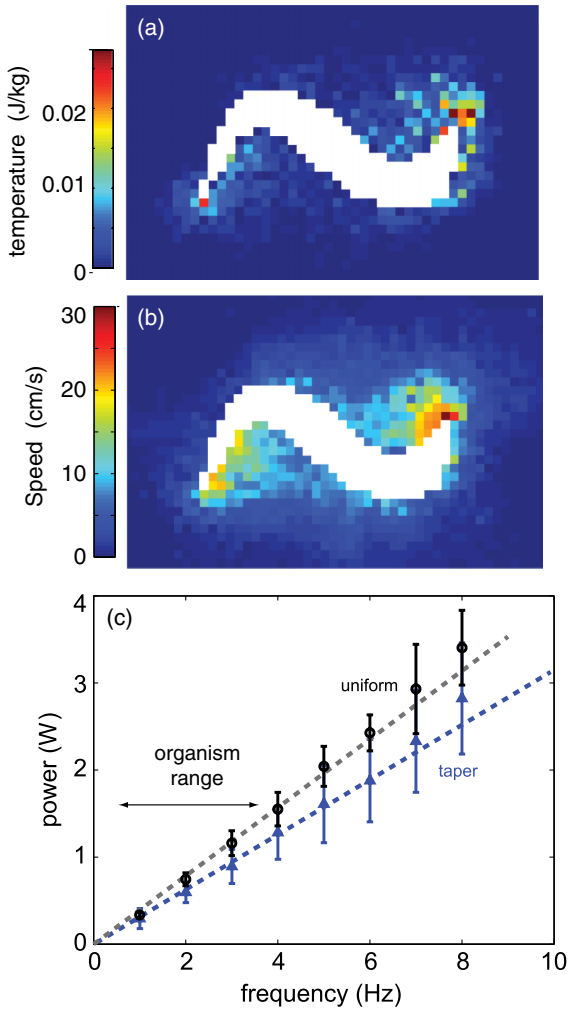

FIG. 9 (color online). Swimming within a localized granular fluid. (a) The granular temperature calculated from particles within cells with dimensions of 0.3 cm (W) by 0.3 cm (L) by 1.6 cm (H). (b) Flow field in which color represents the instantaneous speed of particles (averaged within the same cells as in the temperature calculation). $A/\lambda = 0.22$, $f = 4$ Hz. (c) The peak power required to swim within the granular frictional fluid vs frequency for a tapered and uniform body shape. Adapted from Ding *et al.*, 2012.

forces revealed that, in accord with the rod drag measurements (Fig. 2), the force pattern during swimming was also insensitive to swimming speed. Thus during sand swimming friction dominates the interaction of the animal with its environment (Ding *et al.*, 2012).

Combining these results gives a picture of sand swimming: the head breaks material which flows near the body and whose fluid resistance is speed independent, unlike that of a true fluid. We therefore refer to such locomotion as swimming in a "frictional fluid." Interestingly, within the range of physiologically relevant swimming frequencies (< 4 Hz), the tapered body reduces power demands only by 30%; this is in accord with previous studies that found that "streamlining" in granular drag has a small effect relative to what can be achieved in true fluids (Albert *et al.*, 2001). We studied the effects of particle-particle and particle-body friction on the performance of a granular swimmer [a robot, described below and in Maladen, Ding, Umbanhowar, and Goldman (2011)] and found that over a range $< 0.05 < \mu < 0.5$ the particle-particle friction coefficient does not affect swimming speed, but increasing particle-body μ decreases swimming speed. Further work, however, is needed to elucidate the effects of friction on the properties of the frictional fluid and its effects on locomotion.

B. Resistive force theory

The simulation allows for detailed modeling of granular swimming but does not readily provide insight into the fundamental force balances that produce the observed mechanics. Neither does it admit to simplified analysis. In this regard it functions at the level of computational fluid dynamics simulations of swimming in true fluids (Tytell *et al.*, 2010). Therefore, to better understand sand swimming, inspired from the simulation prediction that swimming takes place within a local frictional fluid, and that inertial effects are small, we developed a theoretical approach, inspired by the resistive force theory (RFT) pioneered for swimming at low Reynolds number by Taylor (1951) and Gray and Hancock (1955).

In our granular RFT, the body of the organism is partitioned into infinitesimal square elements along its length; see Fig. 10. When moving relative to the medium, each element experiences resistive thrust and drag forces. Resolving these forces into perpendicular ($F_\perp$) and parallel ($F_\parallel$) components, the net forward force on an element is

$$\delta F_x = \delta F_\perp \sin\theta - \delta F_\parallel \cos\theta, \tag{2}$$

where θ is the angle between the direction of the average velocity of the organism and the instantaneous orientation of the infinitesimal element. θ increases with the oscillation amplitude and can be obtained by differentiating the fit sinusoidal wave equation (2) (Maladen, Ding, Kamor *et al.*, 2011). Integrating stresses over the length and width of the body (and head) and setting the integral to zero predicts forward swimming speed at a given frequency, assuming resistive forces dominate inertial forces and assuming a so-called drag anisotropy such that the ratio $F_\perp/F_\parallel > 1$. Since at biologically relevant swimming speeds (0–0.4 m/s) force is independent of speed (Wieghardt, 1975; Maladen *et al.*, 2009), the force on an element can be characterized as a function of only the *direction* of the velocity relative to its orientation. As the entry angle of the animal is small (< 30°), we approximate the motion of the animal as occurring in the horizontal plane.

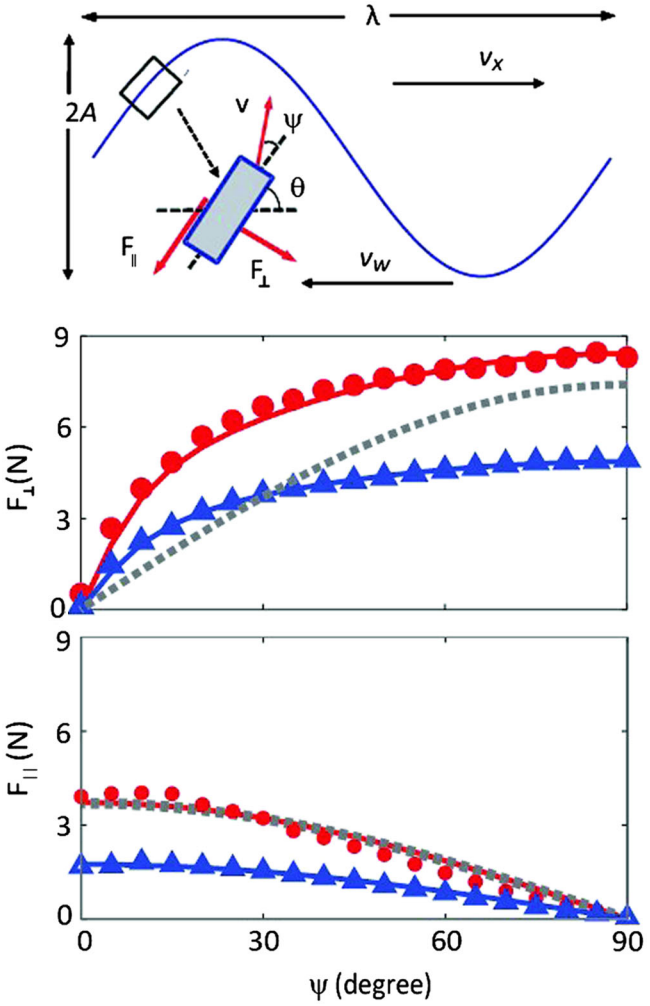

FIG. 10 (color online). Schematic diagram showing forces on an element of an undulatory locomotor, used for granular resistive force theory (RFT) calculations. In the granular RFT, the object has a square cross-sectional shape similar to that in the DEM simulation and forces are computed by integrating stresses over surface elements. (Lower panels) Empirical granular drag force relations used in the granular resistive force theory. Circles and triangles indicate $\phi = 0.62$ and $\phi = 0.58$, respectively. The dashed curve indicates forces for drag of a slender object in a low Reynolds number fluid, scaled to match in magnitude $F_\parallel$ for $\phi = 0.62$. Adapted from Maladen *et al.*, 2009.

The missing ingredients are the force relations $F_\perp$ and $F_\parallel$ as a function of the angle of each element relative to its instantaneous velocity direction ψ; see Fig. 10. Since resistive force laws in GM were not available, we measured in both experiment (Maladen *et al.*, 2009) and simulation (Maladen, Ding, Kamor *et al.*, 2011) the forces on rods with comparable cross sections to the animal body as the rods were dragged through GM at a fixed depth (similar to Fig. 7). These are shown in Fig. 10 and, as in other granular drag experiments, were speed independent. The angular dependence of the force laws in GM resembles the forces generated in a Newtonian fluid at low Reynolds number: $F_\perp$ increases and $F_\parallel$ decreases

with increasing angle between the velocity of the rod and its longitudinal axis. However, while the functional forms of the forces in low Re can be approximated as sines and cosines, in GM, they do not have these simple functional forms; while $F_{\parallel}$ somewhat resembles that of low Re, $F_{\perp}$ rises more rapidly than its low Re counterpart. We presently do not have an explanation for the rapid rise in $F_{\perp}$, although DEM simulation indicates that it is related to a solidlike pile-up of grains near the surface, a consequence of the materials ability to maintain finite stress before shearing.

We next assumed that we could approximate stresses on elements by dividing the measured forces by rod areas (Maladen *et al.*, 2009; Maladen, Ding, Kamor *et al.*, 2011). Inputting these forces into the granular RFT gave good prediction of speed versus frequency and η but when compared to DEM, it overpredicted swimming speeds in 3 mm particles; see Fig. 11. We posit that this is due to an effect of hysteresis in granular drag. This is supported by comparison of reaction forces in DEM and RFT (Ding *et al.*, 2012): the instantaneous force predicted by the granular force relations is typically larger than that measured in the DEM, particularly near reversals of body elements. Recently, we discovered that in drag experiments (Ding *et al.*, 2012) on rods the force on an oscillating rod rises to its predicted steady-state value over a certain distance. We hypothesize that this transient effect results in overestimates by the RFT of thrust forces and thus produces the overestimation in η by the RFT observed in Fig. 11. We also posit that this effect dominates the discrepancy between RFT and DEM, rather than the segmental interaction effects seen in fluids (Lauga and Powers, 2009) (that is, the assumed segmental force being independent of movement of nearby segments). We note that in recent experiments, in which the direction of motion does not reverse, RFT predicts locomotion of a legged robot on the surface of GM to within a few percent (Li, Zhang, and Goldman, 2013).

The granular RFT gives insight into how thrust and drag forces conspire to generate swimming within sand. First, as in all swimmers, drag forces are anisotropic; thus the net force [Eq. (2)] on an element moving appropriately through the GM can be greater than zero, and a pattern of self-deformation (like a traveling sinusoidal wave) can generate forward movement [see supplemental information in Maladen, Ding, Kamor *et al.* (2011) for details]. Since the drag anisotropy is larger in GM ($> 3:1$) than in fluids in which it is at most $\approx 2:1$, consequently, thrust is relatively larger in GM compared to that in a fluid at low Reynolds number. This explains the higher η observed for sandfish (≈ 0.5) compared to noninertial low Re swimmers in fluids (≈ 0.2). We note that in smaller particles the animal can reach higher speeds (using higher frequencies) in more closely packed materials; we do not know the reason for this. It could be related to the change in the rheology of intrusion in closely packed material relative to loosely packed material [for a discussion of force and flow fields during drag in granular media, see Gravish, Umbanhowar, and Goldman (2010)] or the slight dependence of force on drag speed (Fig. 2) in closely packed material.

The RFT also suggests that ϕ does not affect η because both thrust and drag scale similarly with changes in volume fraction. That is, the functional forms for $F_{\perp}$ and $F_{\parallel}$ are similar for both ϕ tested. In the RFT calculation, the ratio of thrust to drag plays the dominant role in determining forward speed [see supplemental information in Maladen, Ding, Kamor *et al.* (2011) for details]. An alternative explanation is that the material disturbed by the sandfish rapidly evolves to the same ϕ_c, the critical volume fraction (Gravish, Umbanhowar, and Goldman, 2010; Umbanhowar and Goldman, 2010), and thus the body of the organism always moves within GM of the same ϕ.

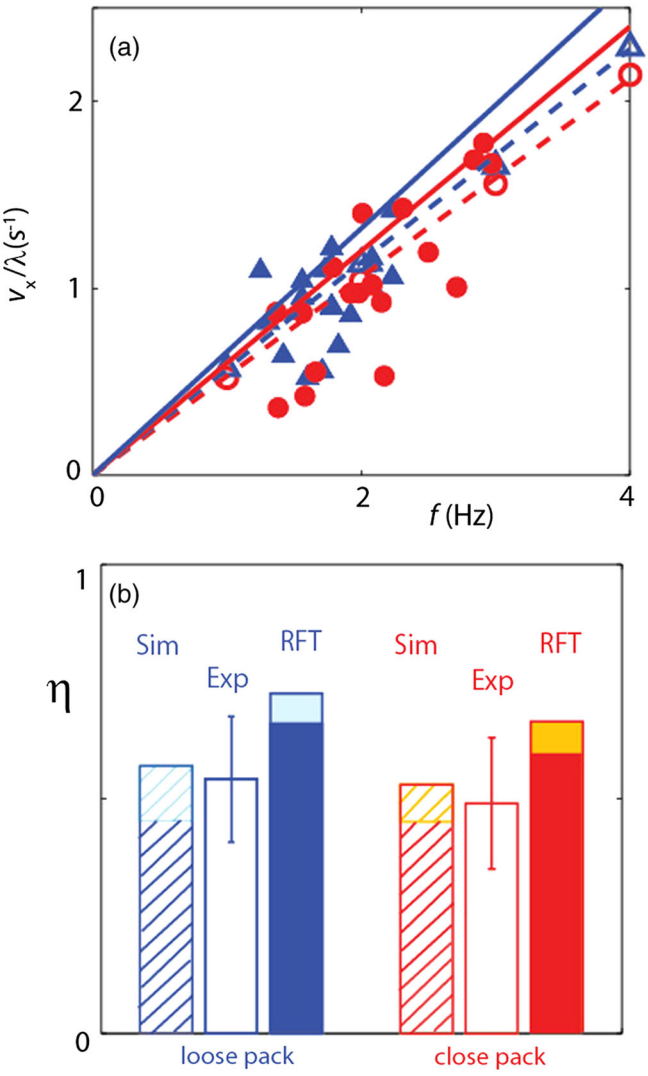

FIG. 11 (color online). (a) Sandfish average forward swimming speed vs undulation frequency in 3 mm diameter glass particles compared to DEM simulation and RFT predictions with $A/\lambda = 0.22$. Solid circles and triangles denote closely and loosely packed states, respectively. (b) Wave efficiency η for animal, DEM simulation, and RFT. Ranges in DEM and RFT predictions indicate a tapered and uniform body. Adapted from Maladen, Ding, Kamor *et al.*, 2011.

C. Robot modeling

The modeling approaches described thus far are useful in part because they allow us to readily vary parameters. However, both approaches rely on empirical models of interaction with the environment. To remedy this, we created a robotic physical model (Maladen, Ding, Kamor *et al.*, 2011), an approach which is becoming popular in the field of

organismal biomechanical modeling since environmental interaction does not need to be modeled. Our sand-swimming robot [see Fig. 12(a)] was created from six connected servo motors (HSR 5980SG digital servos) whose angular position could be computer controlled to generate different time and spatially varying waveforms. Two layers of "skin" prevented the GM (composed of 6 mm diameter ABS plastic particles) from interfering with the motors. We found that when an approximation of a traveling sinusoidal wave was commanded to propagate from head to tail, like the sandfish, the robot swam forward within the GM and its forward speed increased linearly with its undulation frequency; see Fig. 12(b). The robot did not move forward as fast or with the same η as the animal; its $\eta \approx 0.34$ was significantly below that of the animal. We hypothesized that the number of segments (for a fixed length device) affected both η and the forward speed of the device. Increasing the number of segments in the experiment was inconvenient due to motor limitations, so we used our DEM simulation to create a numerical sandfish robot; the simulation agreed well with experiment, further confirming its utility; see Fig. 12(b). Increasing the number of segments in the robot simulation revealed that the device swam faster and with greater η until $N \approx 15$, where η plateaued near $\eta \approx 0.5$, comparable to animal experiment. [see the inset of Fig. 12(b)]. We used the granular RFT to predict η for a smooth profiled undulator of similar size to the sandfish robot and obtained $\eta = 0.56$ (shaded band). Thus, the robot experiments validated our modeling approaches and our modeling of the sandfish.

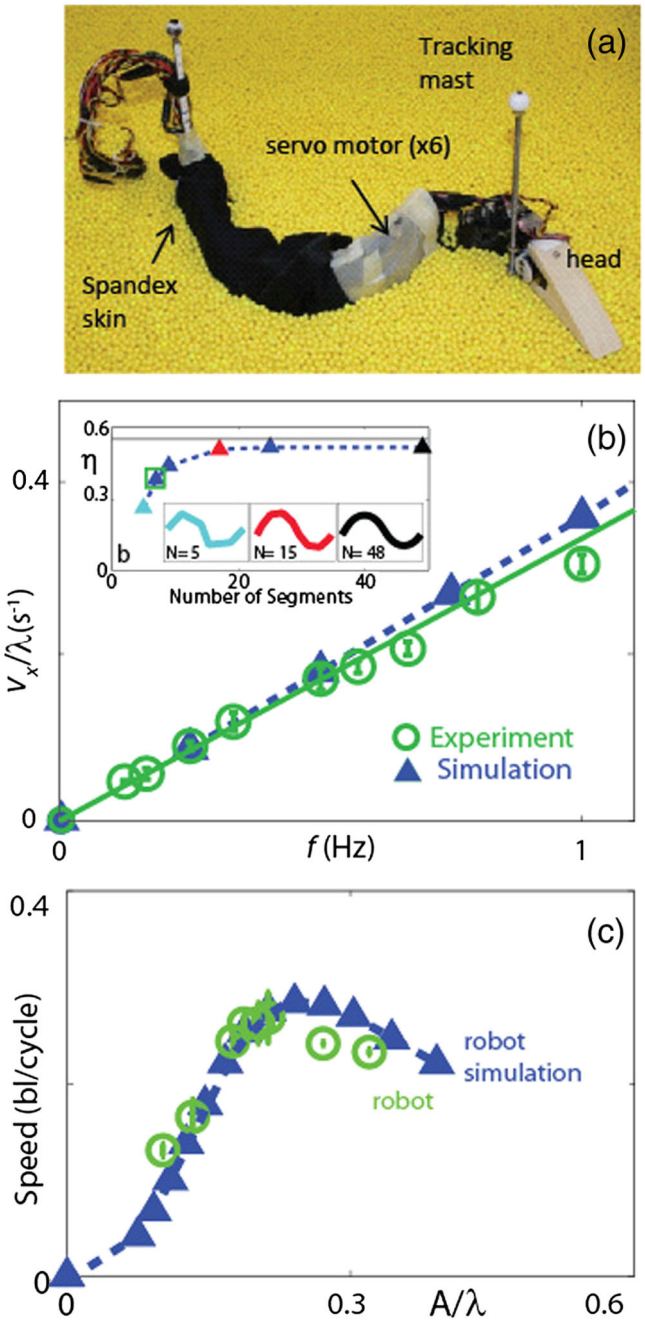

FIG. 12 (color online). Swimming in a robot physical model of the sandfish in experiment and DEM simulation. (a) The robot resting on a bed of 6 mm plastic spheres. The robot consists of six servomotors controlled to execute an approximate sinusoidal wave with fixed A/λ. (b) Speed (scaled by wavelength) vs f in experiment (circles) and DEM simulation (triangles). Inset: Wave efficiency (calculated in DEM simulation) increases with increasing smoothness. (c) Speed in body lengths per cycle vs A/λ in experiment (circles) and DEM simulation (triangles). Frequency is 0.5 Hz. Adapted from Maladen, Ding, Kamor *et al.*, 2011.

VIII. SAND SWIMMING AS A CONTROL TEMPLATE

The models allow variation of parameters that are challenging (or impossible) to vary in biological experiment. For example, in the experiment we noticed that the animal maintained a waveform with fixed A/λ, independent of conditions (compaction, depth). The model gave an explanation for this. We varied the amplitude of the body wave while maintaining the shape as a single period sinusoid and the body at a fixed length (since the animal is inextensible). The simulation and robot experiments revealed that at intermediate amplitudes the swimming speed was maximized [see Figs. 12(c) and 13(a)] and mechanical cost of transport [energy per mass used to travel a distance, see Tucker (1975)] was minimized [see Fig. 13(a)]. Since the animal uses a wave of $A/\lambda \approx 0.2$ during its rapid dive into the granular medium, and only for a few undulation cycles, we hypothesize that the animal attempts to advance a maximal number of body lengths per undulation cycle during its escape behavior.

The RFT explains the optimum in speed in Fig. 13(a) as a competition between an increase in η [Fig. 13(b)] results from larger amplitude [see supplemental information in Maladen, Ding, Kamor *et al.* (2011) for details of the calculation] and a decrease in λ that is a result of an inextensible body and increasing A [Fig. 13(b)]. We can express forward speed in body lengths per second as v_x/fL. Since we measure in the animal that $v_x = \eta f \lambda$, this expression can be written as $\eta \times \lambda/L$ which expresses forward speed in body lengths per undulation cycle. [1]

[1]To better compare with RFT we also developed a body which did not vary in cross section and had flat ends, a "uniform" body. We found that the RFT overestimated speed by ≈20%. We attribute this to the overestimation of thrust related to body reversals; see Ding *et al.* (2012). However, further work is needed to determine if this (or perhaps segmental interaction effects) is the dominant source of the discrepancy between RFT and DEM.

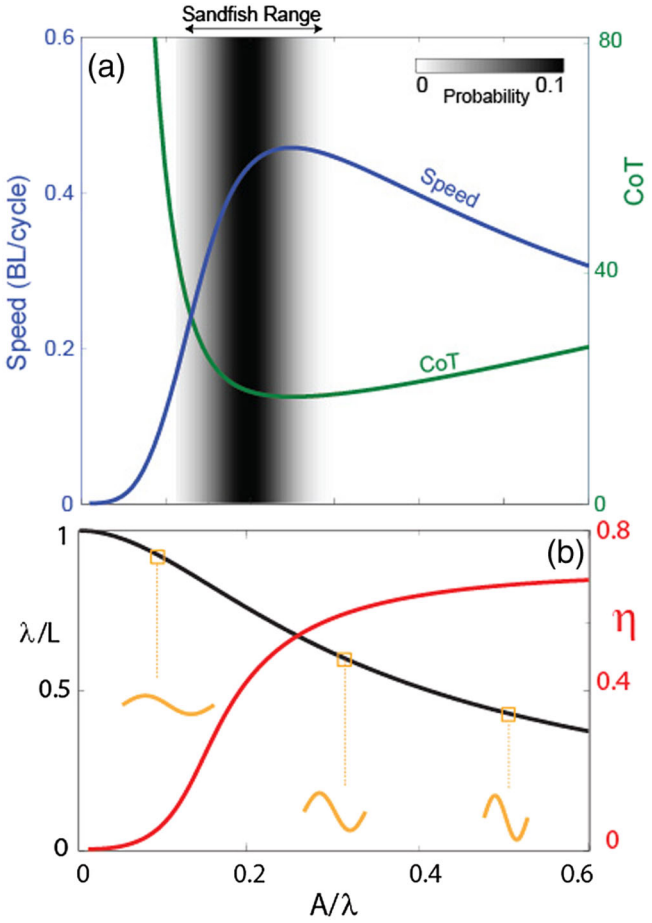

FIG. 13 (color online). Optimal swimming in sand and its origin. (a) RFT predictions of speed in body lengths per cycle ("speed" curve) and weight specific mechanical cost of transport (CoT) vs A/λ. The vertical shaded region shows a probability distribution of A/λ measured in the sandfish by Maladen *et al.* (2009) and Sharpe, Ding, and Goldman (2013), where the darker shading indicates more animals were observed operating with the corresponding spatial form. The average spatial form is $A/\lambda = 0.2 \pm 0.04$. (b) Predictions of η (colored curve) vs A/λ and λ/L (black curve) vs A/λ from RFT.

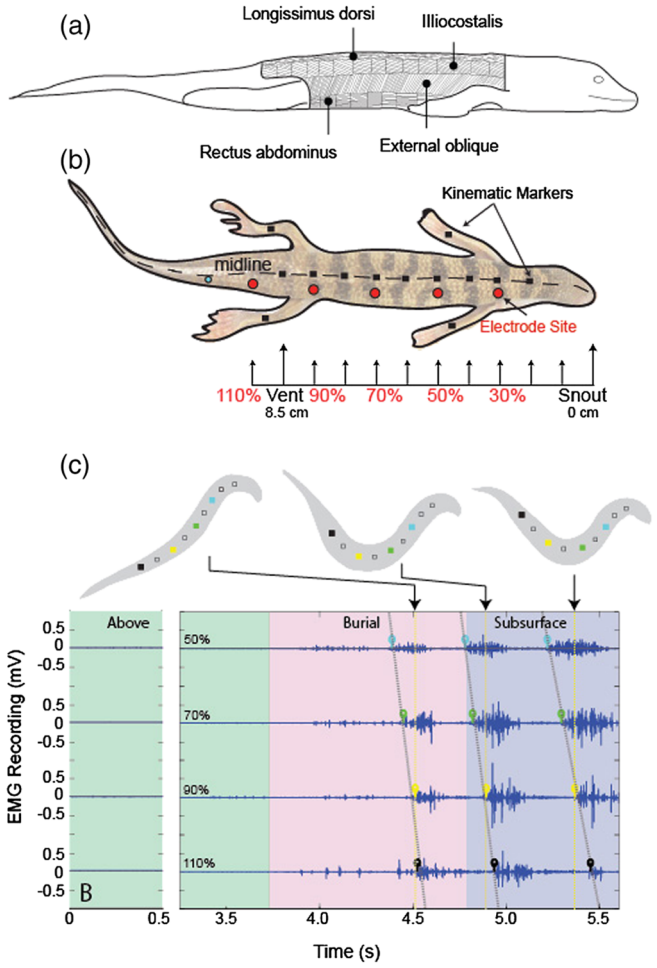

FIG. 14 (color online). A wave of muscle activity accompanies the wave of body bending during subsurface swimming. (a) Diagrammatic representation of some superficial axial musculature in the sandfish. (b) Electromyography (EMG) setup with representation of the location of the EMG electrode implantation sites (circles) and the opaque markers (squares) attached to the exterior right dorsal side. (c) Top images show dorsal views of the sandfish body position during burial and subsurface movements. Each image corresponds to the onset of the 0.7 EMG burst (circles). Below, EMG recordings are shown at 0.5, 0.7, 0.9, and 1.1 SVL (snout-vent length) locations. Colored stems indicate the onset of the EMG burst. Adapted from Sharpe, Ding, and Goldman, 2013.

The previous results imply that the animal actively controls its muscles to target the waveform—such a result indicates that this wave could be a "template" for neuromechanical control, discussed by Full and Koditschek (1999). To investigate this, we recognize that all animals that use undulatory locomotion do so by contracting muscles—such muscle contraction can be measured by recording voltages developed in the muscle tissue. This technique is called electromyography (EMG) (Loeb and Gans, 1986) and has been widely used to compare activation strategies during locomotion (Gillis, 1996, 1998). EMG gives a window into the action of the nervous system during movement and as such can allow tests of movement control models.

To test this, we performed the first measurements of muscle activity during sand swimming. To do so, we developed a technique to simultaneously record EMG from a set of back muscles in the sandfish synchronized with x-ray imaging; see Sharpe, Ding, and Goldman (2013) for details. We used bipolar hook electrodes implanted in the epaxial musculature on one side of the body at several locations from head to slightly beyond the base of the tail; see Figs. 14 and 15(a). When the vertebrate muscle contracts, a potential is developed within the muscle (creating measurable voltages typically of the order of 100 μV); these voltages were sent to an amplifier through fine wires bundled that were attached to the base of the tail (to prevent a signal due to the movement of the electrodes). Like other undulatory swimmers (Gillis, 1998), muscles on alternate sides of the body contract such that a wave of electrical activity is present during undulation (see Fig. 14). We found that the activation timing of the wave propagated at a speed greater than that of the wave of bending of the body. The phenomenon leads to an advancing phase of

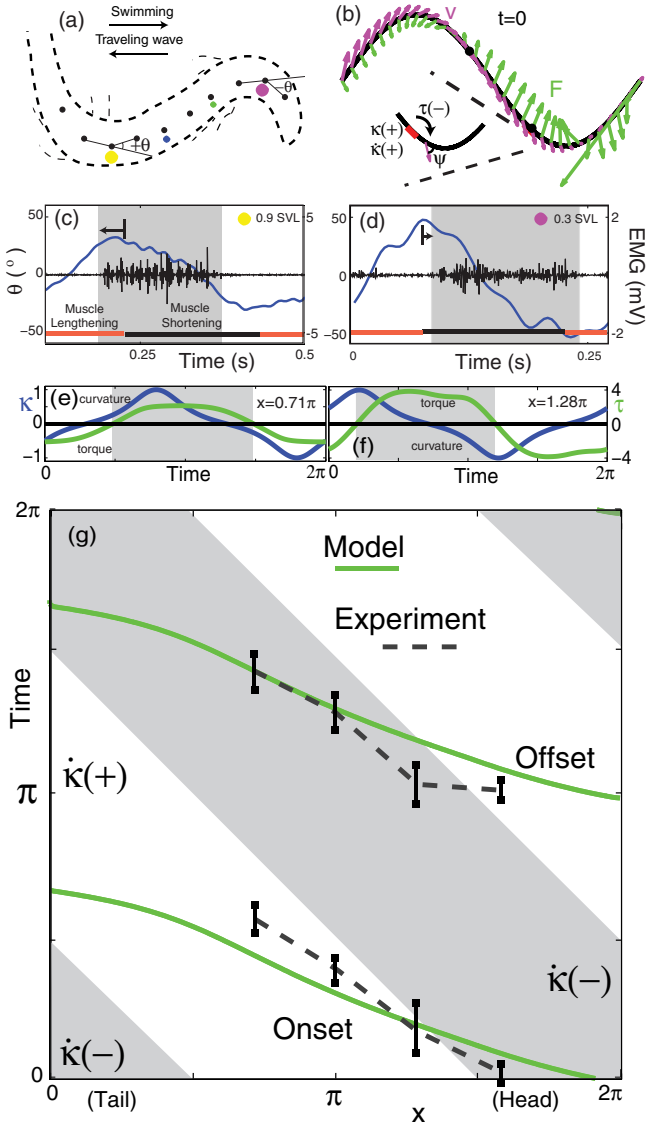

FIG. 15 (color online). The timing of muscle activation relative to body curvature during sand swimming. (a) The trace of a sandfish during sand swimming. Opaque markers (circles) are attached to the exterior midline to facilitate tracking. Colored dots represent implanted electrodes on the right side of the body. (b) Diagram of the model. V arrows represent velocity and F arrows represent forces from the medium. The inset shows the signs of the torque (τ), the curvature (κ), and the rate of change of curvature ($\dot{\kappa}$) at approximately 0.6 body length. Negative τ corresponds to no muscle activation on the right side of the body (thick line). ψ indicates the angle between the segment axis and its velocity. (c), (d) EMG recordings at 0.9 and 0.3 SVL, respectively, during sand swimming. The shaded regions indicate muscle activation. The line shows the measured angle between consecutive markers [see (a)]. Arrows indicate the difference in time between the onset of muscle activation and maximal convexity, the "neuromechanical phase lags." (e), (f) The curvature, torque, and the predicted muscle activation (gray shaded regions) from the RFT model at two representative points indicated by black dots in (b). (g) The predicted onset and offset of muscle activation from the model compared to EMG measurements from the sandfish experiment (black error bars indicate standard deviations). The shaded areas indicate the periods of negative $\dot{\kappa}$. $A/\lambda = 0.22$. Adapted from Ding *et al.*, 2013.

activation relative to the curvature toward the tail and is called the "neuromechanical phase lags" [see Figs. 15(c) and 15(d)]. Neuromechanical phase lags are observed in all swimmers in true fluids (Gillis, 1998), although the lags differ in different species.

Remarkably, we found that the RFT predicted the neuromechanical phase lags in the sandfish [see Fig. 15(g)] with no fitting parameters and with only the assumption (confirmed by animal body bending tests) that the body bending forces were small relative to the forces required to push body segments through the medium (Ding *et al.*, 2013). This result implies that the muscle activity in the back which drives the movement (targeting of a neuromechanical control template which optimizes speed and minimizes energy use) emerges as a consequence of the coupled animal-substrate system. Further, because of the relative simplicity of the waveform used by the sandfish, the lack of inertial effects in the medium, and the applicablity of RFT, we were able to pinpoint the source of the difference in wave speeds of the EMG to curvature waves; such an analysis is challenging in swimmers (like the lamprey) (McMillen, Williams, and Holmes, 2008; Tytell *et al.*, 2010) moving in more complex fluid environments (such that fluid inertia is important). A simplified version of our model reveals that the neuromechanical phase lags arise from a combination of synchronized torques from distant points on the body and local traveling torques [see Ding *et al.* (2013) for the development of the model].

IX. CONCLUSIONS AND OUTLOOK

In this Colloquium, I have described our biological observations of a sand-swimming lizard and demonstrated that the theoretical, numerical, and robotic tools we have developed can explain some features of its locomotion, including optimal kinematic and energetic performance and the timing of neuromuscular control signals. I have also pointed out areas of granular physics that require a more fundamental understanding, and how the sand-swimming problem forces examination of these. Our work is a starting point in the investigation of animal movement in dry granular media and other fluidizing terrestrial ground. Tools like those described can provide insight into morphological features (like body and head shapes) of the myriad organisms that inhabit such environments (not only within terrain, but also during movement on substrates that flow and deform). Surprisingly, the seemingly strange system of an animal "swimming" in sand can give insight into experiment and theory comparison for nervous system control of movement more generally. Further, our recent use of geometric methods (Hatton *et al.*, 2013) reveals that granular swimming can be described in a general gauge potential framework first introduced by Shapere and Wilczek (1987); this analysis reveals that sand swimming bears similarities to swimmers in viscous fluid regimes, broadening, again, the applicability of the sand-swimming system. Questions of reversibility and the presence or absence of the "scallop" theorem (Purcell, 1977) should be investigated.

While the majority of the work done by physicists on biological systems has occurred at the cellular and molecular scales (Nelson, 2008; Phillips, 2009), as noted by Nelson

(2008), studies at the organism scale present biological physics challenges across length and time scales—from biophysics of muscle motor proteins to dynamical systems analysis of gaits (Golubitsky *et al.*, 1999). Locomotion on complex terrestrial ground also requires advances in understanding of the physics of substrate rheological properties of "soft materials" like sand, wet soil, leaf litter, and bark—many of these substrates encountered by animals (and robots) are not yet described by equations of motion like those that describe fluids. In summary, it remains a challenge to discover how such subsystems integrate to generate the emergent behavior of movement in complex environments. Many interesting and important questions [within locomotion biology as well as ecology (Nathan *et al.*, 2008) and paleontology (Clack, 2002)] can be addressed only with a quantitative understanding driven by the interplay of biological experiment, robotics, numerical simulation, and theory. Recently we have discovered that RFT works well on above-ground granular locomotion (Li, Zhang, and Goldman, 2013), broadening the range of questions that can be addressed.

Finally, addressing a larger point, while many of the constituent components of locomotor systems are understood, there is not yet an integrated understanding of how locomotion *emerges* from the many degrees of freedom, active and passive nonlinearly coupled or coordinated electrical, chemical, and mechanical systems that compose animals. For example, although a large literature exists on the neurobiology of locomotor behaviors (Grillner, 1985), many recent studies suggest that mechanical systems, for example, in the interaction of the animal's musculoskeletal system and the environment, also play an important role in the control of locomotion (Daniel and Tu, 1999; Full and Koditschek, 1999; Dickinson *et al.*, 2000; Daley *et al.*, 2006; Nishikawa *et al.*, 2007; Ristroph *et al.*, 2010; Ding *et al.*, 2013). And of course even simple locomotor systems can prove challenging to understand: a mechanical 2 degree-of-freedom double pendulum can display chaos (Shinbrot *et al.*, 1992), although if two such pendula are coupled appropriately, such a system can walk stably and seemingly like a human (McGeer, 1990; Collins *et al.*, 2005). I posit that a "physics of moving systems" is needed to discover principles (Bialek, 2012) by which "lifelike" behaviors like movement emerge from complex combinations of nonliving elements. I also expect that robots will play a role in such developments, particularly as models that interact with materials that do not yet have equations of motion. Finally, I propose that (perhaps surprisingly) locomotion in granular material is an excellent system to investigate these issues.

ACKNOWLEDGMENTS

This work was supported by The Burroughs Wellcome Fund Career Award at the Scientific Interface, NSF Physics of Living Systems Grants No. PHY-0749991 and No. PHY-1150760, the Army Research Laboratory (ARL) Micro Autonomous Systems and Technology (MAST) Collaborative Technology Alliance (CTA) under cooperative agreement No. W911NF-08-2-0004 and the Army Research Office under Grant No. W911NF-11-1-0514. I thank Robert J. Full and Ted Pappenfuss for introducing me to sandfish. I thank my students and collaborators, including Yang Ding, Nick Gravish, Chen Li, Ryan Maladen, Sarah Sharpe, and Paul Umbanhowar; they performed the bulk of the work reported here.

REFERENCES

Albert, I., J. Sample, A. Morss, S. Rajagopalan, A. Barabási, and P. Schiffer, 2001, Phys. Rev. E **64**, 061303.
Albert, R., M. Pfeifer, A. Barabasi, and P. Schiffer, 1999, Phys. Rev. Lett. **82**, 205.
Alexander, R. M., 2003, *Principles of Animal Locomotion* (Princeton University Press, Princeton, NJ).
Anderson, P. W., 1972, Science **177**, 393.
Andreotti, B., Y. Forterre, and O. Pouliquen., 2013, *Granular Media: Between Fluid and Solid* (Cambridge University Press, Cambridge, England).
Aristotle, 350 BCE, De motu animalium (http://ebooks.adelaide.edu.au/a/aristotle/motion/). Translated by A. S. L. Farquharson, 1912 (Clarendon Press, Oxford).
Arnold, E. N., 1995, J. Zool. **235**, 351, Pt. 3.
Bagnold, R., 1941, *The Physics of Blown Sand and Desert Dunes*, reprinted in 1954 by Methuen, London.
Becker, L. E., S. A. Koehler, and H. A. Stone, 2003, J. Fluid Mech. **490**, 15.
Bekker, M., 1956, *Theory of Land Locomotion* (The University of Michigan Press, Ann Arbor, MI).
Bialek, W., 2012, *Biophysics: Searching for Principles* (Princeton University Press, Princeton, NJ)..
Bläsing, B., and H. Cruse, 2004, J. Comp. Physiol. A **190**, 173.
Blickhan, R., 1989, J. Biomech. **22**, 1217.
Blickhan, R., and R. J. Full, 1993, J. Comp. Physiol. A **173**, 509.
Borelli, G. A., 1680, De Motu Animalium. Translated as The Movement of Animals, Paul Maquet (Springer-Verlag, Berlin), 1989.
Campbell, C. S., 1990, Annu. Rev. Fluid Mech. **22**, 57.
Cavagna, G. A., N. C. Heglund, and C. R. Taylor, 1977, Am. J. Physiol. **233**, R243.
Childress, S., 1977, *Mechanics of swimming and flying* (Courant Institute of Mathematical Sciences, New York University, New York).
Clack, J., 2002, *Gaining Ground: The Origin and Evolution of Tetrapods* (Indiana University Press, Bloomington, IN).
Clark, A. H., L. Kondic, and R. P. Behringer, 2012, Phys. Rev. Lett. **109**, 238302.
Cofer, D., G. Cymbalyuk, W. J. Heitler, and D. H. Edwards, 2010, J. Exp. Biol. **213**, 1060.
Cohen, N., and J. H. Boyle, 2010, Contemp. Phys. **51**, 103.
Collins, S., A. Ruina, R. Tedrake, and M. Wisse, 2005, Science **307**, 1082.
Cruse, H., T. Kindermann, M. Schumm, J. Dean, and J. Schmitz, 1998, Neural Netw. **11**, 1435.
Daley, M. A., J. R. Usherwood, G. Felix, and A. A. Biewener, 2006, J. Exp. Biol. **209**, 171.
Daniel, T. L., and M. S. Tu, 1999, J. Exp. Biol. **202**, 3415.
Darwin, C., 1897, *The formation of vegetable mould, through the action of worms: with observations on their habits* (Appleton, New York).
Dickinson, M. H., C. T. Farley, R. J. Full, M. A. R. Koehl, R. Kram, and S. Lehman, 2000, Science **288**, 100.
Dickinson, Michael H., Fritz-Olaf Lehmann, and Sanjay P. Sane, 1999, Science **284**, 1954.
Dickinson, W. W., and J. D. Ward, 1994, J. Sediment. Res. **64**, 226.

Ding, Y., N. Gravish, and D. I. Goldman, 2011, Phys. Rev. Lett. **106**, 028001.
Ding, Y., S. S. Sharpe, A. Masse, and D. I. Goldman, 2012, PLoS Comput. Biol. **8**, e1002810.
Ding, Y., S. S. Sharpe, K. Wiesenfeld, and D. I. Goldman, 2013, Proc. Natl. Acad. Sci. U.S.A. **110**, 10123.
Dorgan, K., S. Arwade, and P. Jumars, 2007, J. Exp. Biol. **210**, 4198.
Dorgan, K., P. Jumars, B. Johnson, B. Boudreau, and E. Landis, 2005, Nature (London) **433**, 475.
Edwards, C. A., 1996, *Biology and ecology of earthworms* (Springer, New York), Vol 3.
Ezcurra, E., 2006, *Global Deserts Outlook*, Global Environment Outlook (United Nations Environment Programme).
Ferris, D. P., M. Louie, and C. T. Farley, 1998, Proc. R. Soc. B **265**, 989.
Fish, F. E., 1984, Copeia **1984**, 839.
Frolich, L., and A. Biewener, 1992, J. Exp. Biol. **162**, 107.
Full, R. J., and D. E. Koditschek, 1999, J. Exp. Biol. **202**, 3325.
Gaymer, R., 1971, Nature (London) **234**, 150.
Geng, J., D. Howell, E. Longhi, R. Behringer, G. Reydellet, L. Vanel, E. Clément, and S. Luding, 2001, Phys. Rev. Lett. **87**, 35506.
Gillis, G., 1998, J. Exp. Biol. **201**, 949.
Gillis, G. B., 1996, American Zoologist **36**, 656.
Gillis, G. B., 1997, J. Exp. Biol. **200**, 767.
Goldman, D., and P. Umbanhowar, 2008, Phys. Rev. E **77**, 021308.
Goldman, D. I., T. S. Chen, D. M. Dudek, and R. J. Full, 2006, J. Exp. Biol. **209**, 2990.
Golubitsky, M., I. Stewart, P. L. Buono, and J. J. Collins, 1999, Nature (London) **401**, 693.
Gravish, N., D. Monaenkova, M. A. D. Goodisman, and D. I. Goldman, 2013, Proc. Natl. Acad. Sci. U.S.A. **110**, 9746.
Gravish, N., P. B. Umbanhowar, and D. I. Goldman, 2010, Phys. Rev. Lett. **105**, 128301.
Gray, J., and G. J. Hancock, 1955, J. Exp. Biol. **32**, 802.
Gray, J., and H. Lissman, 1964, J. Exp. Biol. **41**, 135.
Gray, J. S., and M. Elliott, 2009, *Ecology of marine sediments : from science to management* (Oxford University Press, New York), 2nd ed.
Grillner, S., 1985, Science **228**, 143.
Hatton, R. L., Y. Ding, H. Choset, and D. I. Goldman, 2013, Phys. Rev. Lett. **110**, 078101.
Hill, G., S. Yeung, and S. A. Koehler, 2005, Europhys. Lett. **72**, 137.
Hirose, S., 1993, *Biologically Inspired Robots: Serpentile Locomotors and Manipulators* (Oxford University Press, New York).
Hlldobler, B., and E. O. Wilson, 1990, *The Ants* (Belknap Press, Cambridge, MA).
Holmes, P., R. J. Full, D. Koditschek, and J. Guckenheimer, 2006, SIAM Rev. **48**, 207.
Howell, D., R. P. Behringer, and C. Veje, 1999, Phys. Rev. Lett. **82**, 5241.
Ijspeert, A., A. Crespi, D. Ryczko, and J. Cabelguen, 2007, Science **315**, 1416.
Irschick, D., and B. Jayne, 1999, J. Exp. Biol. **202**, 1047.
Jaeger, H. M., S. R. Nagel, and R. P. Behringer, 1996a, Rev. Mod. Phys. **68**, 1259.
Jaeger, H. M., S. R. Nagel, and R. P. Behringer, 1996b, Phys. Today **49**, No. 4, 32.
Jayne, B. C., and D. J. Irschick, 1999, J. Exp. Biol. **202**, 143.
Jenkins, J., and M. Richman, 1985, Arch. Ration. Mech. Anal. **87**, 355.
Juarez, G., K. Lu, J. Sznitman, and P. E. Arratia, 2010, Europhys. Lett. **92**, 44002.
Jung, S., 2010, Phys. Fluids **22**, 031903.
Katsuragi, H., and D. J. Durian, 2007, Nat. Phys. **3**, 420.
Koditschek, D. E., R. J. Full, and M. Buehler, 2004, Arthropod Structure and Development **33**, 251.
Korff, W. L., and M. J. McHenry, 2011, J. Exp. Biol. **214**, 122.
Korta, J., D. Clark, C. Gabel, L. Mahadevan, and A. Samuel, 2007, J. Exp. Biol. **210**, 2383.
Kuo, A. D., J. M. Donelan, and A. Ruina, 2005, Exercise and Sport Sciences Reviews **33**, 88.
Lauder, G., and E. Tytell, 2006, Fish Physiology **23**, 425.
Lauder, G. V., E. J. Anderson, J. Tangorra, and P. G. A. Madden, 2007, J. Exp. Biol. **210**, 2767.
Lauga, E., and T. R. Powers, 2009, Rep. Prog. Phys. **72**, 096601.
Lee, J., and H. Herrmann, 1993, J. Phys. A **26**, 373.
Lejeune, T. M., P. A. Willems, and N. C. Heglund, 1998, J. Exp. Biol. **201**, 2071.
Li, C., S. T. Hsieh, and D. I. Goldman, 2012, J. Exp. Biol. **215**, 3293.
Li, C., P. Umbanhowar, H. Komsuoglu, and D. Goldman, 2010, Exp. Mech. **50**, 1383.
Li, C., P. Umbanhowar, H. Komsuoglu, D. Koditschek, and D. Goldman, 2009, Proc. Natl. Acad. Sci. U.S.A. **106**, 3029.
Li, C., T. Zhang, and D. I. Goldman, 2013, Science **339**, 1408.
Loeb, G. E., and C. Gans, 1986, *Electromyography for Experimentalists* (University of Chicago Press, Chicago, IL).
Maladen, R., Y. Ding, A. Kamor, P. Umbanhowar, and D. Goldman, 2011, J. R. Soc. Interface **8**, 1332.
Maladen, R., Y. Ding, C. Li, and D. Goldman, 2009, Science **325**, 314.
Maladen, R., Y. Ding, P. B. Umbanhowar, and D. I. Goldman, 2011, Int. J. Robotics Research **30**, 793.
McGeer, T., 1990, Int. J. Robotics Research **9**, 62.
McMillen, T., T. Williams, and P. Holmes, 2008, PLoS Comput. Biol. **4**, e1000157.
Moritz, C. T., and C. T. Farley, 2003, Proc. R. Soc. B **270**, 1741.
Mosauer, W., 1932, Copeia **1932**, 72.
Murphy, R., 2014, *Disaster Robotics* (MIT Press, Cambridge, MA).
Nathan, R., W. M. Getz, E. Revilla, M. Holyoak, R. Kadmon, D. Saltz, and P. E. Smouse, 2008, Proc. Natl. Acad. Sci. U.S.A. **105**, 19052.
Nedderman, R., 1992, *Statics and kinematics of granular materials* (Cambridge University Press, Cambridge, England).
Nelson, P., 2008, *Biological Physics* (W. H. Freeman, New York).
Nishikawa, K. *et al.*, 2007, Integrative and Comparative Biology **47**, 16.
Phillips, R., 2009, *Physical biology of the cell* (Garland Science, New York).
Poschel, T., 2005, *Computational granular dynamics : models and algorithms* (Springer-Verlag, Berlin).
Purcell, E., 1977, Am. J. Physiol. **45**, 3.
Rapaport, D. C., 2004, *The art of molecular dynamics simulation* (Cambridge University Press, Cambridge, England), 2nd ed.
Ristroph, L., A. J. Bergou, G. Ristroph, K. Coumes, G. J. Berman, J. Guckenheimer, Z. J. Wang, and I. Cohen, 2010, Proc. Natl. Acad. Sci. U.S.A. **107**, 4820.
Robins, B., 1742, *New Principles of Gunnery*, reprinted in 1972 by Richmond Publishing Co. Ltd.
Schmitt, J., M. Garcia, R. C. Razo, P. Holmes, and R. J. Full, 2002, Biol. Cybern. **86**, 343.
Seyfarth, A., H. Geyer, M. Gunther, and R. Blickhan, 2002, J. Biomech. **35**, 649.
Shapere, A., and F. Wilczek, 1987, Phys. Rev. Lett. **58**, 2051.
Sharpe, S. S., Y. Ding, and D. I. Goldman, 2013, J. Exp. Biol. **216**, 260.

Shattuck, M. D., C. Bizon, J. B. Swift, and H. L. Swinney, 1999, Physica (Amsterdam) **274A**, 158.
Shen, X. N., and P. E. Arratia, 2011, Phys. Rev. Lett. **106**, 208101.
Shinbrot, T., C. Grebogi, J. Wisdom, , and J. A. Yorke, 1992, Am. J. Phys. **60**, 491.
Spagna, J. C., D. I. Goldman, P.-C. Lin, D. E. Koditschek, and R. J. Full, 2007, Bioinsp. Biomim. **2**, 9.
Spence, A. J., S. Revzen, J. Seipel, C. Mullens, and R. J. Full, 2010, J. Exp. Biol. **213**, 1907.
Sponberg, S., and R. J. Full, 2008, J. Exp. Biol. **211**, 433.
Tan, M.-L., and I. Goldhirsch, 1998, Phys. Rev. Lett. **81**, 3022.
Taylor, G., 1951, Proc. R. Soc. A **209**, 447.
Taylor, J., 1952, Proc. R. Soc. A **214**, 158.
Terzaghi, K., 1943, *Theoretical soil mechanics* (Wiley, New York).
Trueman, E. R., 1970, J. Exp. Biol. **53**, 701.
Tschinkel, W. R., 2006, *The Fire Ants* (Belknap Press, Cambridge).
Tucker, V. A., 1975, Am. Sci. **63**, 413.
Tytell, E., C. Hsu, T. Williams, A. Cohen, and L. Fauci, 2010, Proc. Natl. Acad. Sci. U.S.A. **107**, 19832.
Umbanhowar, P., and D. I. Goldman, 2010, Phys. Rev. E **82**, 010301.
Vogel, S., 1994, *Life in Moving Fluids* (Princeton University Press, Princeton, NJ)..
Weber, J. N., B. K. Peterson, and H. E. Hoekstra, 2013, Nature (London) **493**, 402.
Wieghardt, K., 1975, Annu. Rev. Fluid Mech. **7**, 89.
Willert, C. E., and M. Gharib, 1991, Exp. Fluids **10**, 181.
Wilson, E. O., 1998, *Consilience: The Unity of Knowledge* (Knopf, New York), distributed by Random House, 1st ed.
Winter, A. G., R. L. H. Deits, and A. E. Hosoi, 2012, J. Exp. Biol. **215**, 2072.
Wolfe, D., 2002, *Tales from the Underground: A Natural History of Subterranean Life* (Perseus, Cambridge, MA).
Wong, J. Y., 1989, *Terramechanics and off-road vehicles* (Elsevier, New York).
Wright, C., A. Johnson, A. Peck, Z. McCord, A. Naaktgeboren, P. Gianfortoni, M. Gonzalez-Rivero, R. Hatton, and H. Choset, 2007, in *IEEE/RSJ International Conference on Intelligent Robots and Systems, 2007. IROS 2007* (IEEE, New York), pp. 2609–2614.
Zajac, F. E., 1993, J. Biomech. **26**, 109.